Journal of Biomedical Optics

SPIEDigitalLibrary.org/jbo

Feasibility of intrafraction whole-body motion tracking for total marrow irradiation

Manju Sharma
Troy Dos Santos
Nikolaos P. Papanikolopoulos
Susanta Kumar Hui

SPIE

Feasibility of intrafraction whole-body motion tracking for total marrow irradiation

Manju Sharma,[a] Troy Dos Santos,[a] Nikolaos P. Papanikolopoulos,[b,c] and Susanta Kumar Hui[a,c,d]
[a]University of Minnesota Medical School, Department of Therapeutic Radiology–Radiation Oncology, MMC 494–420 Delaware Street SE, Minneapolis, Minnesota 55455
[b]University of Minnesota Medical School, Department of Computer Science and Engineering, MMC 494–420 Delaware Street SE, Minneapolis, Minnesota 55455
[c]University of Minnesota Medical School, Biomedical Engineering, MMC 494–420 Delaware Street SE, Minneapolis, Minnesota 55455
[d]University of Minnesota Medical School, Biophysical Sciences and Medical Physics MMC 494–420 Delaware Street SE, Minneapolis, Minnesota 55455

Abstract. With image-guided tomotherapy, highly targeted total marrow irradiation (TMI) has become a feasible alternative to conventional total body irradiation. The uncertainties in patient localization and intrafraction motion of the whole body during hour-long TMI treatment may pose a risk to the safety and accuracy of targeted radiation treatment. The feasibility of near-infrared markers and optical tracking system (OTS) is accessed along with a megavoltage scanning system of tomotherapy. Three near-infrared markers placed on the face of a rando phantom are used to evaluate the capability of OTS in measuring changes in the markers' positions as the rando is moved in the translational direction. The OTS is also employed to determine breathing motion related changes in the position of 16 markers placed on the chest surface of human volunteers. The maximum uncertainty in locating marker position with the OTS is 1.5 mm. In the case of normal and deep breathing motion, the maximum marker position change is observed in anterior–posterior direction with the respective values of 4 and 12 mm. The OTS is able to measure surface changes due to breathing motion. The OTS may be optimized to monitor whole body motion during TMI to increase the accuracy of treatment delivery and reduce the radiation dose to the lungs. [DOI: 10.1117/1.3575645]

Keywords: megavoltage scanning system; near-infrared maker; motion tracking; total marrow irradiation.

Paper 10417R received Jul. 22, 2010; revised manuscript received Mar. 11, 2011; accepted for publication Mar. 21, 2011; published online May 20, 2011.

1 Introduction

As radiation therapy continues to advance, more conformal radiation treatment has been made possible. In conformal radiation treatment, the radiation dose conforms to the shape of the target while sparing sensitive neighboring areas of the body from high radiation delivery. Recently, total marrow irradiation is being explored as a part of the hematopoietic cell transplantation (HCT) preparative regimen.[1–4] We have developed methodologies for selective total marrow irradiation (TMI) using tomotherapy,[5,6] which has a potential to replace the current method of total body irradiation (TBI). Tomotherapy is an image guided radiation therapy machine that delivers conformed radiation helically around the patient. It has an onboard megavoltage computed tomography (MVCT) detector which supports 3D image guidance for patient setup.[7–13] TMI treatment using tomotherapy is critically dependent on accurate patient positioning.[14,15] During the development and initial clinical experiences of TMI treatment, we acknowledged potential challenges and concerns such as: (a) risk of geographic miss if proper precautions are not taken during precise delivery, (b) hour long treatment time, and (c) the lack of "closed loop" technology that would provide feedback to the irradiation system notifying of an unsafe patient position so as to disable the primary radiation beam to allow for adjustments to be made in the patient position during treatment.

Different strategies are used to monitor the patient's body motion between treatment fractions (interfraction) or during (intrafraction) treatment. One obvious strategy is to immobilize the patient using frame-based treatment such as an alpha cradle.[16,17] Though immobilization techniques improve treatment delivery, they cannot be used to correct for various involuntary patient body movements during treatment such as breathing motion. Various methods have been proposed, investigated, and implemented to track patient (or surface) motion or target motion. These include x-ray tracking,[18] electronic portal imaging,[19] ultrasound tracking,[20] 4DCT,[21] and camera-based optical tracking systems.[22,23] These modalities in turn have inherent limitation such as ultrasound is limited to image soft tissue, and as a result would not be useful to track whole body. A predominant limitation of x-ray and 4DCT is the radiation exposure as even under optimal conditions they induce a dose per imaging session. The portal imaging being a two- dimensional (2D) projection method contains effects of superimposed structures between radiation source and detector. It shows large density differences as an example while distinguishing air and bone from soft tissue background. This poses a problem for tumor verification as most tumors are made of soft tissue. As such, the optical motion tracking system holds promise because it does not involve

Address all correspondence to: Susanta K Hui, University of Minnesota Medical School, Department of Therapeutic Radiology – Radiation Oncology, 420 Delaware Street SE, Mayo Mail Code 494, Minneapolis, Minnesota 55455. Tel: 612–626-4484, Fax: 612–626-7060, E-mail: huixx019@umn.edu.

1083-3668/2011/16(5)/058002/8/$25.00 © 2011 SPIE

radiation exposure. Moreover, it is a noninvasive methodology that does not require surgical implants of fiducial markers and can be used to track the patient's whole body position, a necessity for ensuring the correct alignment of patients receiving TMI treatment.[23]

Tracking multiple points on the body surface is an informative method to know about the articulation of segments. Using the point tracking algorithm as a base, body segments such as boney anatomy, the head or the breastplate can be fairly well approximated as rigid bodies individually as they do not deform much, but not with respect to each other. This method may be used to collect information about the location and orientation of individual body parts throughout the treatment process, which may provide meaningful feedback to medical personnel to reposition patients. This manuscript aims to report the feasibility of a near-infrared (NIR) marker- based optical tracking system (OTS) to monitor body motion during highly confined TMI treatment. The present work describes: (a) the calibration of NIR optical tracking system; (b) the comparison of OTS with an onboard three-dimensional (3D) MVCT scanning system used for pre-treatment setup verification during TMI treatment; (c) characterize the OTS to measure changes in the marker position associated with deep and normal breathing motion in human volunteers.

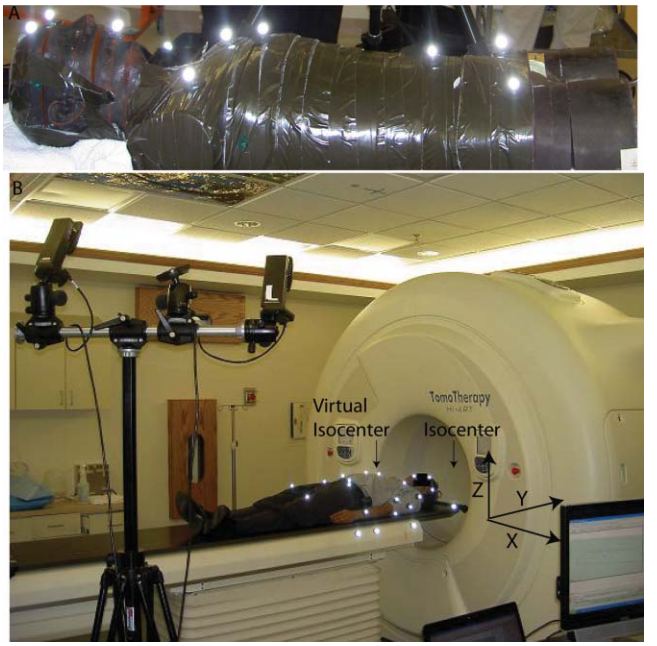

Fig. 1 An overview of the OTS. (a) Rando phantom with near-infrared markers. (b) Two of the six cameras used for tracking the infrared markers and a human volunteer to show the schematic representation.

2 System Overview

In the present study, we used two different patient positioning systems, the OTS and the onboard MVCT imaging system. Written below is a brief description of the two systems.

2.1 *Optical Tracking System*

2.1.1 *OTS setup*

The OTS consists of a spectroscopic camera system with NIR reflective markers obtained from Motion Analysis Corp. (MAC, Santa Rosa, California). Small rubber sphere markers with reflective tape are attached to a rando phantom (The Phantom Laboratory, Salem, New York) [Fig. 1(a)] and human volunteer [Fig. 1(b)] with an adhesive on the base. Each marker is a 12.5-mm diameter spherical rubber ball painted with NIR reflective powder. The cameras have a ring of light emitting diodes (LEDs) positioned around the lens. The NIR markers reflect the light from the LEDs back to the cameras. The cameras capture intensity images, which are then thresholded, and the centroid of each high-intensity connected region is found by a triangulation method. Each camera is calibrated (details given in Sec. 3.2.1) and the location of the center in each camera's image plane is used to determine the 3D location of the detected markers. The entire stereoscopic marker detection system returns a set of 3D marker locations at a rate of 60 Hz.

2.1.2 *Motion data capture and analysis*

The captured motion data is saved in the format of track row column (.trc) and hierarchical translation and rotation (.htr2) in the Eva real-time software (EVaRT) (MAC, Santa Rosa, California). The .trc files containing translational motion data are in ascii format and can be imported into Microsoft Excel to allow basic editing which involves data cleaning and smoothing of the discontinued points. The position data for each marker is organized into three columns per marker (X, Y, and Z position) with each row being a new frame. The position data is relative to the global coordinate systems of the capture volume and the position values are in the same units used for calibration.

2.2 *Tomotherapy and the MVCT Imaging System*

The Tomotherapy has a 6-MV linear accelerator mounted on a ring gantry to deliver radiation in a helical manner.[24–26] The patient lies on the table which then moves through the rotating ring gantry. The tomotherapy uses the International Electrotechnical Commission (IEC) gantry coordinate system (X, Y, Z) as shown in Fig. 1(b).[24,27] During the treatment, the patient is placed on the Tomotherapy couch at the virtual isocenter taken at the intersection of the gantry axis with the axial CT slice containing the point of calculation. This is done for initial laser based alignment. For radiation delivery and MVCT image scans couch moves 70 cm into the bore (Y translation). After each image scan, the couch moves back to virtual isocenter position. In tomotherapy, a linear array of 738 xenon gas detectors and a radiation source with an average energy of 1.36 MeV are used to generate a 3D MVCT image with a field of view of 40 cm. Three different MVCT scanning modes, viz., fine, normal, and coarse, can be used to scan the patient with a slice thickness of 2, 4, and 6 mm, respectively. The treatment planning CT [kilovoltage computed tomographic (kVCT) image from the CT scanner] is superimposed on the MVCT images prior to radiation delivery. The rigid body image registration method is used to match two 3D image sets (kVCT and MVCT) based on anatomical features and tumor locations.[28] The patient positioning errors acquired by the registration process are used in adjusting the patient to reduce day to day misalignment during radiation treatment.

3 Methods

Figure 2(a) shows a flowchart of total marrow irradiation process with anticipated addition to monitor real time body motion (bold). Figure 2(b) shows a flowchart of an OTS feasibility experiment. To track the motion changes in the rando phantom three series of experiments are conducted.

3.1 *Calibration of the Optical Tracking System*

An initial calibration of the NIR markers and the camera arrangement is done using a dynamic 3D calibration method. We use a wand with three markers arranged in a row at a known distance. The wand is moved around until the measurement space is covered which in the present study is the tomotherapy treatment couch. The combined field of view is calibrated by sweeping the wand in all possible directions while the spectroscopically arranged six cameras track the points on the wand. This process generally takes from a few seconds to a couple of minutes depending on the system's detailed requirements. In the present study, it took a few minutes to track a broader area (120 cm × 50 cm) covering the tomotherapy bench as shown in Fig. 1(b). The calibration of OTS involves measuring the deviations from known distances between the markers on the wand as measured by the cameras with the EVaRT. Using known distance values, an error approximation algorithm averages the position of each point based on the data gathered by each camera for each frame and calculates an error by which the cameras track a point. This is done for the total number of frames (frame frequency n = 60 Hz) used while collecting data on the wand movements, and then averaged. The collected data is analyzed in Microsoft Excel to determine standard deviation of the average error values for each frame. For further reference, this data will be referred to as optical data.

3.2 *Measurement and Comparison of Translation Change in Marker Position*

The parameters obtained from the calibration procedure (Sec. 3.1) are stored and used for the transformation of image coordinates into 3D marker coordinates. As a result, it is crucial to keep the cameras at the same position throughout the data collection. For evaluating the efficiency of the OTS in locating the position of NIR markers, we glued three NIR markers on the face of a rando phantom. As shown in Fig. 1(a), two markers are placed on the forehead to measure head motion and third marker is placed on the chin to measure motion in the lower jaw and mandible. Placement of three markers is designed to measure head and neck (H&N) skeleton movement. This design also helps to correct any misalignment in pitch (rotation along Y axis), commonly noticed during H&N patient localization for H&N cancer treatment. Without changing the spectroscopic arrangement of cameras, the rando phantom is positioned on the tomotherapy treatment bench. The various steps involved in the evaluation of the OTS are mentioned below.

3.2.1 *Measurement of the initial location of markers*

After aligning the rando phantom, the MVCT scan is performed three times (in three scanning modes viz. fine, normal, and coarse). Optical data is collected for each MVCT scan. This optical data is stored as the reference optical data for the respective scanning mode. The other optical data collected in Secs. 3.2.2 and 3.2.3 is compared with this reference optical data.

3.2.2 *Measurement of translational change in marker position*

Next, in a series of trials, we manually shifted the rando phantom in a vertical direction by increasing the height of the couch (IEC + "Z direction") by Ztr = 10, 30, and 50 mm, where Ztr is the translational shift in the vertical direction. For each position of the rando head we collected the OTS data and took three scans (fine, normal and coarse) as mentioned in Sec. 3.2.1.

3.2.3 *Comparison of OTS and MVCT registration-based marker location systems*

After each MVCT scan, we used the three in-built tomotherapy registration algorithms to determine the realigning corrections; bone, bone/tissue, and full image. In the bone and bone/tissue algorithms threshold values are respectively set to identify bone (i.e., pixels > 1.1 g/cm^3) and bone/tissue (i.e., pixels > 0.3 g/cm^3). The full image-based algorithm has no thresholding for the registration process. The OTS-based detection was repeated several times. Figure 2(d) shows a pictorial representation of the MVCT registration done for the face of the rando phantom. All the MVCT corrections are recorded. The optical data collected in Secs. 3.2.1 and 3.2.2 is compared with the MVCT image registration data.

3.3 *General Tracking of the Markers*

The point tracking algorithm used in the present OTS system works by correlating tracking identification numbers from one frame to the next. Essentially, the tracking number of the nearest point in the last frame is assigned to each point in the current frame. Defining $\ell_{(i,n)}$ to be the location of point i in the current frame and $\ell_{(j,n-1)}$ to be the location of some point j in the previous frame, the tracking identification number associated with $\ell_{(i,n)}$ tracks the identification number associated with the point in the previous frame satisfying $\min_j\{\|\ell_{(i,n)}-\ell_{(j,n-1)}\|_2{}^2\}$. Consistency checks are performed to make sure no identification number is assigned to more than one point in the current frame. If two or more points in the current frame are associated with a single point in the previous frame, only the closest point in the current frame will be associated with it. If a point does not correlate with any point in the previous frame, it is given a new tracking number. A threshold distance d_{thresh} is set for the maximum distance allowed for a point in the current frame to correlate with a point in the previous frame. This value is based upon the expected movement of points between frames. Thus, a point $\ell_{(i,n)}$ will not correlate with any points in the previous frame if $\min_j\{\|\ell_{(i,n)}-\ell_{(j,n-1)}\|_2{}^2\} > d_{\text{thresh}}$. In addition, points that disappear are propagated in their current location for a short duration of time, in the hope that they will reappear shortly. This is done to prevent losing points that temporarily disappear due to a momentary hiccup in the marker detection system. A threshold is manually set as to how many frames a point should be thus propagated since it has last been seen.

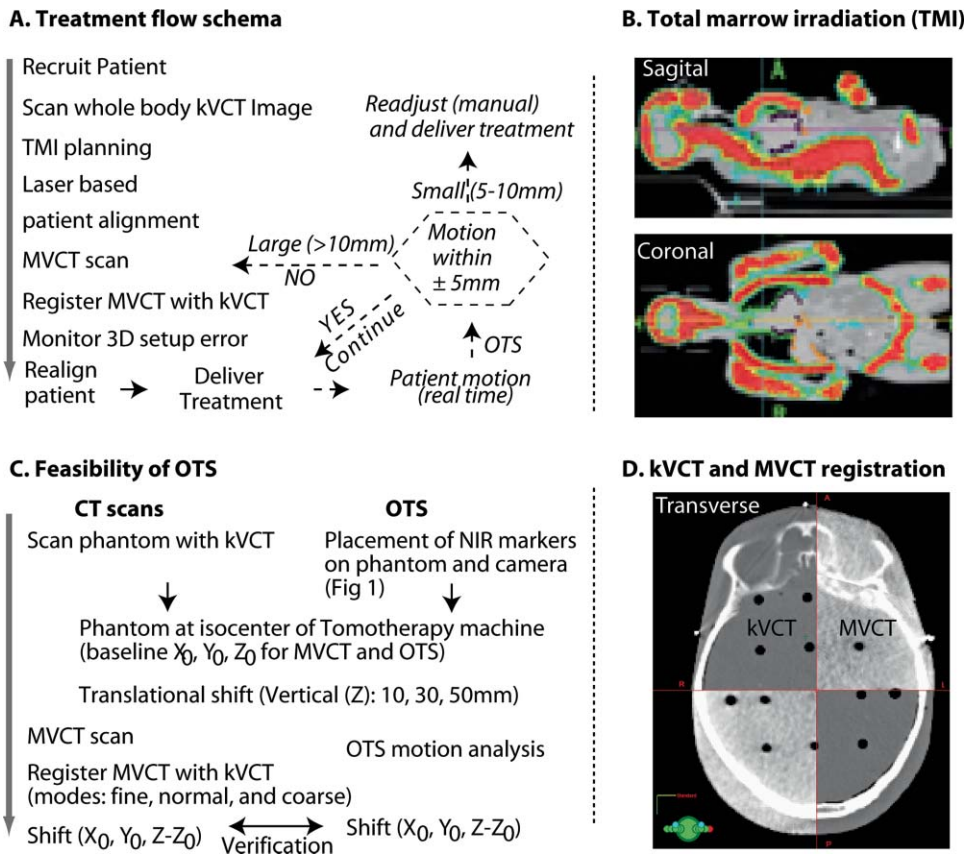

Fig. 2 (a) Treatment schema. Bold (with dotted line) is anticipated integration of real time monitoring of patient body motion for TMI radiation treatment delivery. (b) Validation of OTS system compared with MVCT to measure translation shift of known displacement. (c) The kVCT (dark grey) and MVCT image (light gray) registration of the rando head.

To track body segments such as boney anatomy, the rigid bodies tracked must be manually defined by an operator on captured data sets. A set of points are chosen for each rigid body in an initial frame, which are then tracked with any tracking system such as the OTS system. A rigid body in three dimensions contains six degrees of freedom. The three-dimensional location of the rigid body, $\mathbf{x} = (x, y, z)^T$, is found by taking the mean location of the points associated with it. The locations of each of the constituent points are then found with respect to this center location. Rotation is described by an angle of rotation, θ, and a unit vector around which rotation takes place, $\mathbf{r} = (r_x, r_y, r_z)^T$ in which $\|\mathbf{r}\| = 1$. The Levenberg–Marquardt minimization algorithm is then used to find the best quantities for the set of values $\{x, y, z, r_x, r_y, r_z, \theta\}R$ by minimizing the errors between the expected location of the object points and the detected location of these points within the scene. The Levenberg–Marquardt algorithm is a good choice because the bodies being tracked are not perfectly rigid, but minimum error approximations can still be found.

3.4 *Breathing Motion Analysis Experiment*

To track changes in the body surface as a result of breathing motion, we collected breathing motion data from two human volunteers. A set of 16 NIR markers are placed on the chest in 4×4 mesh like the arrangement shown in Fig. 3. The distance between neighboring NIR markers is kept approximately 10 cm. This creates a 4×4 mesh of roughly 40×40 cm dimension. The markers cover longitudinally most of the chest width-wise and vertically from thoracic to the top of the abdominal surface of the diaphragm. The NIR marker position data is collected for slow and deep breathing motion. The volunteers are asked to hold their breath for a few seconds. The optical data collected during breath hold is taken as reference data (B_{ref}). Volunteers are then told to start the breathing first at normal rate (B_{normal}) and then at deep breathing rate (B_{deep}). During this procedure most of the other motions were controlled by placing the volunteers in an alpha cradle immobilization device. The OTS system records the NIR marker position as the volunteer breathes. The magnitude of normal and deep breathing depends on the comfort level of volunteers. In order to create smooth transitions between different breathing cycles, the human volunteers are asked to perform 2 to 3 min breathing motions. This covers small variations in the breathing process. The noise in the recorded .trc and .htr2 files are removed and discontinued points are smoothed.

4 Results

The calibration of OTS is done with a dynamic linearization technique using the 3 point wand. The Motion Analysis Inc. optical tracking system has been widely used for scientific and

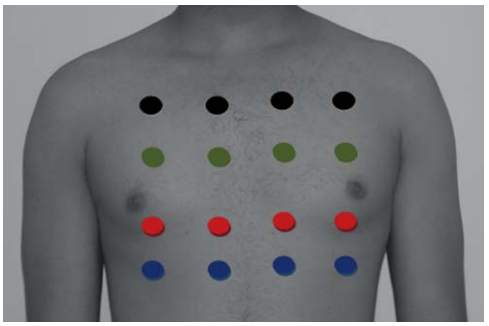

Fig. 3 Pictorial representation of 16 NIR markers placed on a human chest surface to track the breathing motion changes. Different colors are used to distinguish the location of markers.

technical purposes, and reliability and validity has been established and reported in literature.[29] In the present calibration measurements, the average spatial error in locating the NIR marker position is 0.36 mm with a standard deviation of 0.19 mm.

The image registration (as shown in Fig. 2) is done first by using an automatic method followed by a manual check. This is a double check to verify alignment of the MVCT and kVCT images. The shift in *XYZ* coordinates needed to align the MVCT image to the kVCT image is recorded. The NIR marker position changes during the translational motion of the rando phantom in the vertical (z) direction are compared with the

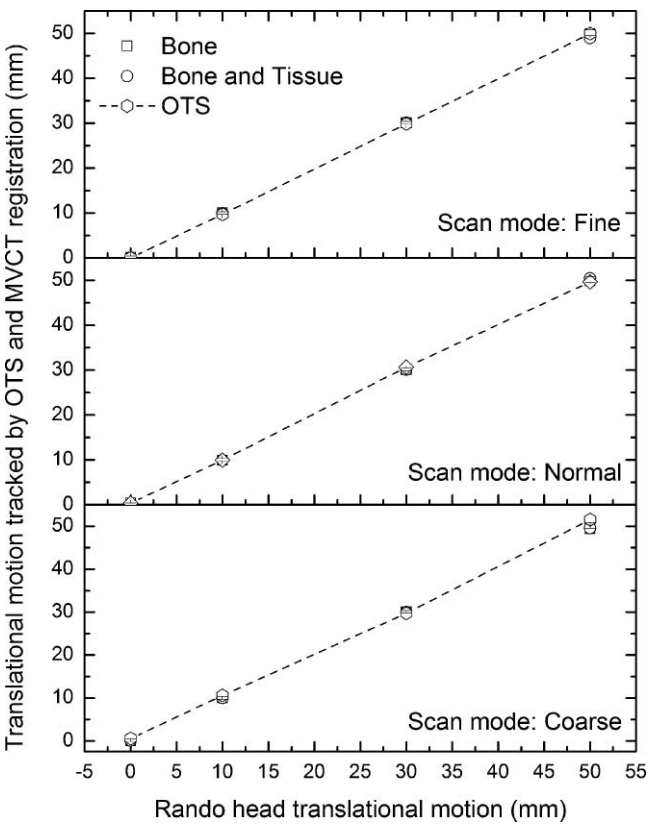

Fig. 4 Tracking translational changes in *Z* using the OTS and MVCT registration methods—bone, bone, and tissue and three different scanning modes—fine, normal and coarse.

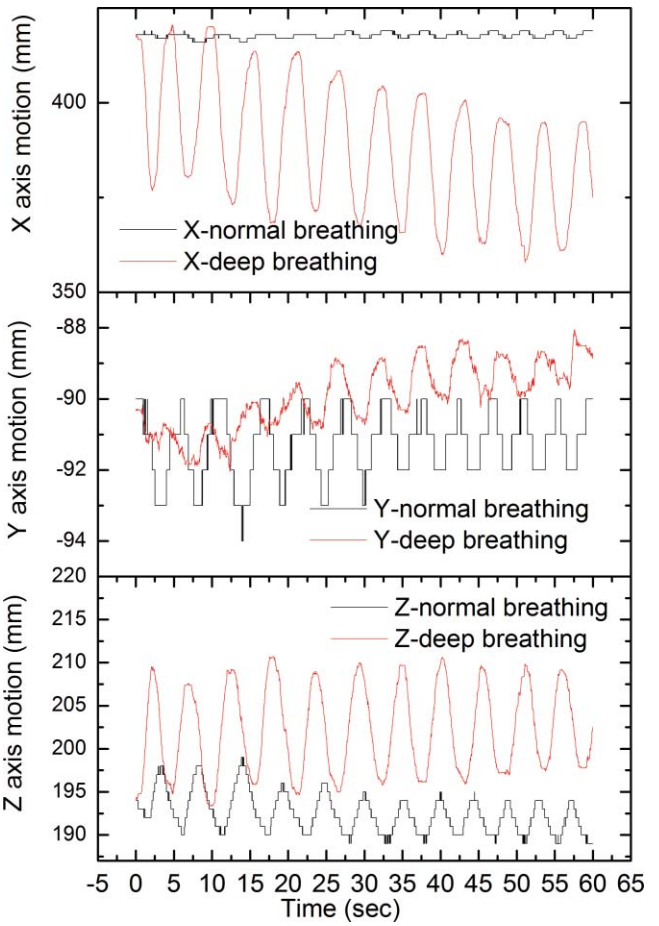

Fig. 5 Breathing motion changes in one marker in the *X*, *Y*, and *Z* directions with respect to time.

OTS system detection uncertainties in Fig. 4 for three scanning modes (fine, normal, and coarse) and two MVCT registration algorithms (bone and bone/tissue). The OTS system shows an uncertainty of ~1.5 mm in the detection of translation shifts in the rando head. The maximum uncertainty in the detection by the MVCT scanning modes is ~2 mm in the case of coarse mode. Better detection accuracy (0.5 to 1.0 mm) is found in fine and normal scanning modes. The average deviation and maximum percentage difference between three registration algorithms are 0.35 mm and 1.9% in the case of the fine scanning mode and 0.34 mm and 1.2% in the case of the normal scanning mode. In the case of the coarse scanning mode, the average deviation is 0.35 mm and maximum percentage difference between three registration algorithms is 6.8%. For a given registration method, the coarse scanning mode reduces the scanning time but it might compromise the measurement accuracy when the structures are small.

We observed the breathing motion changes in the case of two human volunteers. Figure 5 shows the normal and deep breathing motion for time = 1 min in the *XYZ* coordinates measured by one NIR marker. As seen in Fig. 5, each breathing cycle is from 5 to 7 s. The OTS is found to be capable of tracking the correlation between the timing of maximum inspiration and expiration time points. To better visualize the changes in NIR marker position of all 16 markers, we plotted the 3D position and

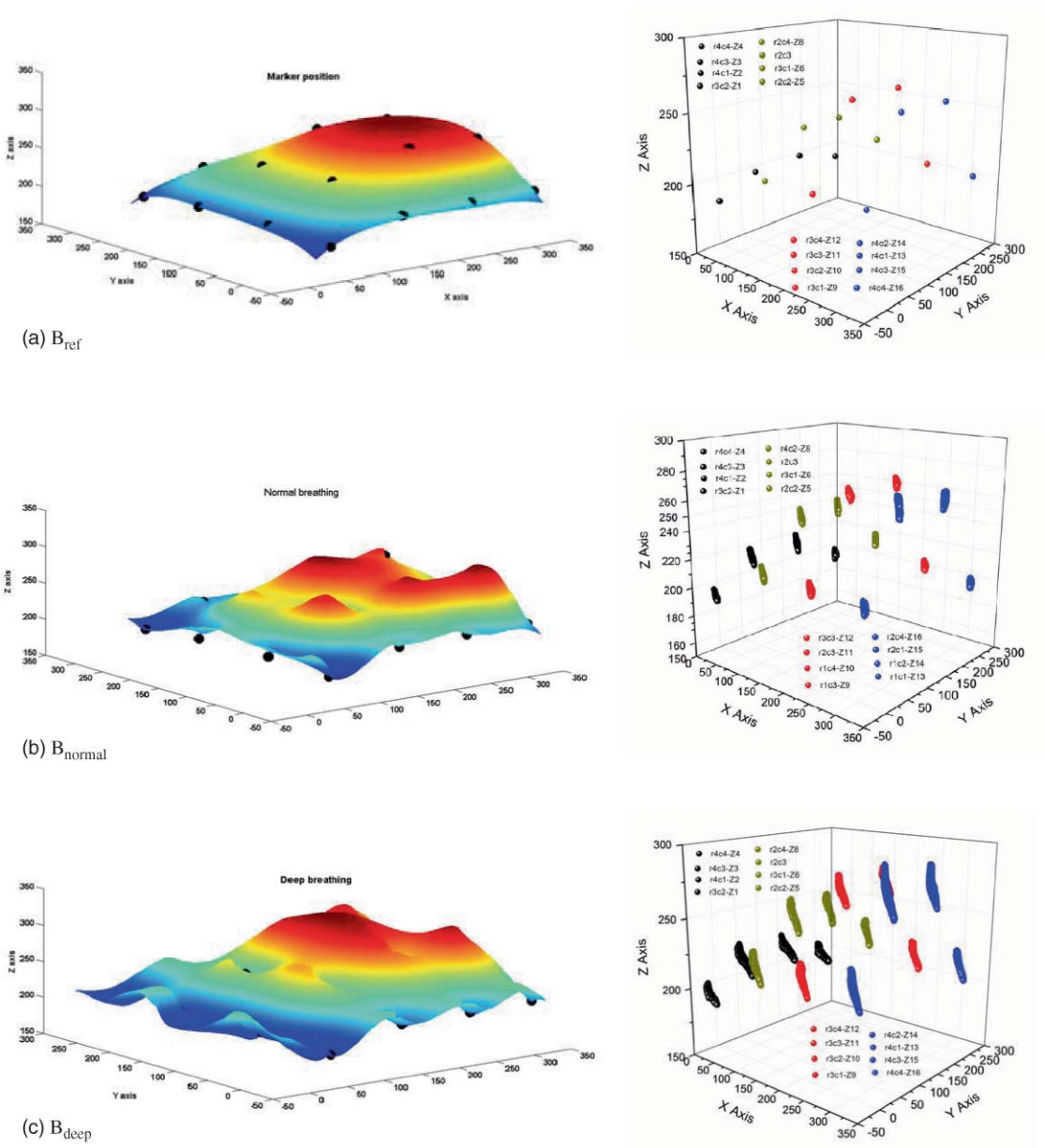

Fig. 6 Surface and 3D scatter plot of change in the position of 16 NIR markers placed on the chest surface of a human volunteer during. (a) the rest phase (B_{ref}); (b) normal breathing (B_{normal}); and (c) deep breathing (B_{deep}).

surface graphs in Figs. 6(a), 6(b), and 6(c), respectively, showing B_{ref}, B_{norm}, and B_{deep}. By keeping the initial position of the markers, the surfaces are constructed for B_{ref}, B_{norm}, and B_{deep} using the grid data and mesh functions of MATLAB (MATLAB 2007b, The Mathworks Inc., Natick, Massachusetts). The grid data function is used with the v4 method. The v4 method uses a Green's function approach and uses a full matrix composed of all the inter point distances to produce smooth surfaces. A 3D scatter plot graph is drawn using Microcal Origin Pro 8.0 (Microcal Software Inc., Northamtom, Masscuhsetts). As shown in Fig. 6, the markers placed near the top of the abdominal surface of the diaphragm show a larger magnitude of change in marker position compared to the markers placed near the mid-thorax and apex. In the case of normal breathing, the maximum shifts in the marker position coordinates in the *X*, *Y*, and *Z* directions are, respectively, 2, 1, and 4 mm. In the case of deep breathing, the maximum changes in *X*, *Y*, and *Z* marker coordinates are 7, 3, and 12 mm, respectivley.

5 Discussion

The feasibility of an NIR marker-based optical tracking system has been demonstrated to monitor rigid and dynamic motion in phantom and in two human volunteers using a tomotherapy treatment unit. The OTS is found to detect changes on par with those of the currently used MVCT scan-based method. The NIR markers used in the present study are equally efficient in light and dark environments compared to the infrared markers, which have a high noise level in light. The current results indicate that OTS should perform well enough to reliably detect 1.5 mm

movement for the human phantom. To get better target positioning accuracy with image registration the fine or normal scanning modes should be used. The use of OTS in tracking patient motion changes during treatment is beneficial in many respects. The OTS may be used in real time while treatment is underway (Fig. 2) and issue alerts if a patient moves significantly; a capability that is not currently present. The on-line approach of the image registration process in tomotherapy prolongs the overall total treatment time when compared to conventional treatments.[30] Increased radiation exposure from multiple MVCT scans, prolong treatment time to incorporate MVCT scans, and its inability to measure real time body motion limits its application in TMI treatment. Due to a narrow field of view (40 cm), often MVCT is not useful to scan extremities (for example, arms) for adult patients. On the other hand, the vision-based acquisition can be performed for the entire body in real time very quickly (within a minute) compared to the MVCT scan method (scanning time $>$ 30 min for whole body scan). The human body is capable of moving into many different positions. As such, it is important to know the extent of movement in different directions. With the OTS it is feasible to track the portions of the body (such as the head and chest) separately. This system will provide information about the alignment for each body portion for the patient's entire body as opposed to monitoring the motion of a small tumor region (few centimeters).[22,23]

Lung toxicity is considered a primary dose-limiting factor for TBI due to increased dose to lungs.[31] One of the main aims for the recently developed total marrow irradiation (TMI) method is to reduce radiation dose to lungs to control lung toxicity.[5,6,32] At present, safety margins around the thoracic bone are kept the same (approximately 1.5 cm) for all directions because of limited knowledge of the directional chest wall motion. Breathing motion data shows a relatively larger variation in the diaphragm, in comparison to the apex and thoracic regions of the chest. A reduced safety margin in the apex and thoracic region may help to reduce radiation dose to the lungs. In the present experiment, we used 16 markers. For 3D lung motion, 58 markers have been considered for reasonable accuracy in estimating lung volume.[33] In the future, 3D chest wall motion measured by the markers will be correlated with variation in lung volume during the breathing cycle using a recently developed 4D CT scanner. Future development will also include the ability to optimize a number of parameters associated with the NIR markers (for example, spatial distance between markers and number of markers) to monitor the whole body motion including pelvis, lower torso, and extremities of the body. An integrated system with automated detection of body motion, feedback to control monitor, and subsequent adjustment of patient or treatment delivery will improve the accuracy of the TMI radiation dose delivery and enhance safety of the treatment delivery. In our clinical TMI treatment, measured rotational shift (by the MVCT-kVCT registration) was less than 1°. Therefore, we have not initiated rotational verification. However, rotational motion will be studied in the future.

We have shown the applicability of the OTS system in tracking changes in rigid and dynamic systems. The OTS system can capture task specific dynamic information and allows extracting a great number of measurements long after the subject has moved. This method can be extended to track other anatomical features such as upper and lower body extremities including arms. The next phase of the project will be able to detect natural features on the patient. Possibilities include use of the scale invariant feature transfer (SIFT),[34] speed-up robust feature (SURF),[35] or other similar features. In addition, coughing or hyperventilation events will also be detected by using a laser source mounted above the patient's abdomen, which provides positional values of the abdominal cross section. Hyperventilation differs from coughing in terms of the displacement of the abdomen. It is possible that a patient maintain the same levels of displacement while hyperventilating, thus the only way to differentiate between normal breathing and hyperventilation is based on the frequency of breathing. For hyperventilation detection, therefore, a filter will be used which emphasizes frequencies above the fundamental breathing frequency of normal breathing, so that if the fundamental frequency drifts to a higher value, which is characteristic of hyperventilation, a detection will be issued. This muscle-movement tracking setup will generate temporal data providing information about points on the abdomen undergoing displacement during the breathing cycle. Tracking these points over time will help us monitor breathing and detect an anomaly during the course of monitoring. A multistage filtering scheme will be used to reduce an inherent noise in the laser data measurements. A spatial smoothing filter is first applied, in which the values of the nearby points in the same horizontal line are averaged. This is based on the notion of smoothness of the patient's abdominal cross section, and emphasizes the fundamental breathing frequency of the patient while eliminating high frequency noise.

6 Conclusions

A noninvasive vision-based optical tracking system is shown to be a feasible option or a second check for measuring body motion within 1.5 mm accuracy and was validated using a 3D MVCT imaging system. Accurate assessment of lung motion in different directions may help to develop patient specific safety margins for radiation treatment delivery. Properly optimized optical tracking systems may be used to monitor whole body motion during TMI treatment delivery to increase accuracy of treatment delivery and reduce radiation dose to lungs.

Acknowledgment

This research was supported by the National Science Foundation (NSF No. CNS-0821474), the Digital Technology Center, and the Medical device grant at the University of Minnesota. This work was also supported by PHS Cancer Center Support Grant No. P30 CA77398. The authors thank Motion Analysis Corporation for providing the motion tracking cameras.

References

1. J. Wong, J. Rosenthal, A. Liu, T. Schultheiss, S. Forman, and G. Somlo, "Image-guided total-marrow irradiation using helical tomotherapy in patients with multiple myeloma and acute leukemia undergoing hematopoietic cell transplantation," *Int. J. Radiat. Oncol., Biol., Phys.* **73**(1), 273–279 (2009).
2. I. J. Lee, J. Seong, C. G. Lee, Y. B. Kim, K. C. Keum, C. O. Suh, G. E. Kim, and J. Cho, "Early clinical experience and outcome of helical tomotherapy for multiple metastatic lesions," *Int. J. Radiation Oncology Biol. Phys.* **73**(5), 1517–1524 (2009).

3. J. Wilkie, H. Tiryaki, B. Smith, J. Roeske, J. Radosevich, and B. Aydogan, "Feasibility study for linac-based intensity modulated total marrow irradiation," *Med. Phys.* **35**(12), 5609–5618 (2008).
4. J. Wong, A. Liu, T. Schultheiss, J. Rosenthal, S. Forman, and G. Somlo, "Reduced acute toxicities with image guided targeted marrow irradiation (tmi) using helical tomotherapy (ht) in patients with multiple myeloma and acute leukemia undergoing hematopoietic cell transplantation (HCT)," *Int. J. Radiat. Oncol., Biol., Phys.* **69**(3S), 17–18 (2007).
5. S. Hui, J. Kapatoes, J. Fowler, D. Henderson, G. Olivera, R. Manon, B. Gerbi, T. Mackie, and J. Welsh, "Feasibility study of helical tomotherapy for total body or total marrow irradiation," *Med. Phys.* **32**(10), 3214–3224 (2005).
6. S. Hui, M. Verneris, P. Higgins, B. Gerbi, B. Weigel, S. Baker, C. Fraser, M. Tomblyn, and K. Dusenbery, "Helical tomotherapy targeting total bone marrow-First clinical experience at the University of Minnesota," *Acta Oncol.* **46**(2), 250–255 (2007).
7. S. K. Hui, R. K. Das, J. Kapatoes, G. Oliviera, S. Becker, H. Odau, J. D. Fenwick, R. Patel, R. Kuske, M. Mehta, B. Paliwal, T. R. Mackie, J. F. Fowler, and J. S. Welsh, "Helical tomotherapy as a means of delivering accelerated partial breast irradiation," *Technol. Cancer Res. Treat.* **3**(6), 639–646 (2004).
8. R. Jeraj, T. R. Mackie, J. Balog, G. Olivera, D. Pearson, J. Kapatoes, K. Ruchala, and P. Reckwerdt, "Radiation characteristics of helical tomotherapy," *Med. Phys.* **31**(2), 396–404 (2004).
9. J. M. Kapatoes, G. H. Olivera, J. P. Balog, H. Keller, P. J. Reckwerdt, and T. R. Mackie, "On the accuracy and effectiveness of dose reconstruction for tomotherapy," *Phys. Med. Biol.* **46**(4), 943–966 (2001).
10. T. R. Mackie, T. Holmes, S. Swerdloff, P. Reckwerdt, J. O. Deasy, J. Yang, B. Paliwal, and T. Kinsella, "Tomotherapy: a new concept for the delivery of dynamic conformal radiotherapy," *Med. Phys.* **20**(6), 1709–1719 (1993).
11. K. J. Ruchala, G. H. Olivera, J. M. Kapatoes, E. A. Schloesser, P. J. Reckwerdt, and T. R. Mackie, "Megavoltage CT image reconstruction during tomotherapy treatments," *Phys. Med. Biol.* **45**(12), 3545–3562 (2000).
12. K. J. Ruchala, G. H. Olivera, E. A. Schloesser, and T. R. Mackie, "Megavoltage CT on a tomotherapy system," *Phys. Med. Biol.* **44**(10), 2597–2621 (1999).
13. J. S. Welsh, M. Lock, P. M. Harari, W. A. Tome, J. Fowler, T. R. Mackie, M. Ritter, J. Kapatoes, L. Forrest, R. Chappell, B. Paliwal, and M. P. Mehta, "Clinical implementation of adaptive helical tomotherapy: a unique approach to image-guided intensity modulated radiotherapy," *Technol. Cancer Res. Treat.* **5**(5), 465–479 (2006).
14. X. Li, X. Qi, M. Pitterle, K. Kalakota, K. Mueller, B. Erickson, D. Wang, C. Schultz, S. Firat, and J. Wilson, "Interfractional variations in patient setup and anatomic change assessed by daily computed tomography," *Int. J. Radiation Oncology Biol. Phys.* **68**(2), 581–591 (2007).
15. T. Bortfeld, S. Jiang, and E. Rietzel, "Effects of motion on the total dose distribution," *Seminars in Radiation Oncology* **14**, 41–51 (2004).
16. C. B. Saw, R. Yakoob, C. A. Enke, T. P. Lau, and K. M. Ayyangar, "Immobilization devices for intensity-modulated radiation therapy (IMRT)," *Med. Dosim.* **26**(1), 71–77 (2001).
17. M. J. Murphy and J. Y. Jin, "Patient immobilization and movement," in *Spine Radiosurgery*, Thieme Medical Publishers, New York (2008).
18. P. Keall, V. Kini, S. Vedam, and R. Mohan, "Motion adaptive x-ray therapy," *Phys. Med. Biol.* **46**(1), 1–10 (2001).
19. W. van Elmpt, L. McDermott, S. Nijsten, M. Wendling, P. Lambin, and B. Mijnheer, "A literature review of electronic portal imaging for radiotherapy dosimetry," *Radiother. Oncol.* **88**(3), 289–309 (2008).
20. A. Hsu, N. Miller, P. Evans, J. Bamber, and S. Webb, "Feasibility of using ultrasound for real-time tracking during radiotherapy," *Med. Phys.* **32**(6), 1500–1512 (2005).
21. T. Zhang, W. Lu, G. Olivera, H. Keller, R. Jeraj, R. Manon, M. Mehta, T. Mackie, and B. Paliwal, "Breathing-synchronized delivery: a potential four-dimensional tomotherapy treatment technique," *Int. J. Radiat. Oncol., Biol., Phys.* **68**(5), 1572–1578 (2007).
22. J. Wilbert, J. Meyer, K. Baier, M. Guckenberger, C. Herrmann, R. Hess, C. Janka, L. Ma, T. Mersebach, and A. Richter, "Tumor tracking and motion compensation with an adaptive tumor tracking system (ATTS): System description and prototype testing," *Med. Phys.* **35**(9), 3911–3921 (2008).
23. T. H. Wagner, S. L. Meeks, F. J. Bova, W. A. Friedman, T. R. Willoughby, P. A. Kupelian, and W. Tome, "Optical tracking technology in stereotactic radiation therapy," *Med. Dosim.* **32**(2), 111–120 (2007).
24. T. R. Mackie, J. Balog, K. Ruchala, D. Shepard, S. Aldridge, E. Fitchard, P. Reckwerdt, G. Olivera, T. McNutt, and M. Mehta, "Tomotherapy," *Seminars in Radiation Oncology* **9**, 108–117 (1999).
25. J. N. Yang, T. R. Mackie, P. Reckwerdt, J. O. Deasy, and B. R. Thomadsen, "An investigation of tomotherapy beam delivery," *Med. Phys.* **24**(3), 425–436 (1997).
26. J. Balog, T. R. Mackie, D. Pearson, S. Hui, B. Paliwal, and R. Jeraj, "Benchmarking beam alignment for a clinical helical tomotherapy device," *Med. Phys.* **30**(6), 1118–1127 (2003).
27. J. P. Gibbons, K. Smith, D. Cheek, and I. Rosen, "Independent calculation of dose from a helical TomoTherapy unit," *J. Appl. Clin. Med. Phys.* **10**(1), 103–119 (2009).
28. S. Boswell, W. Tomé, R. Jeraj, H. Jaradat, and T. R. Mackie, "Automatic registration of megavoltage to kilovoltage CT images in helical tomotherapy: an evaluation of the setup verification process for the special case of a rigid head phantom," *Med. Phys.* **33**, 4395 (2006).
29. T. Svoboda, D. Martinec, and T. Pajdla, "A convenient multicamera self-calibration for virtual environments," *Presence: Teleoperators & Virtual Environments* **14**(4), 407–422 (2005).
30. P. Bijdekerke, D. Verellen, K. Tournel, V. Vinh-Hung, F. Somers, P. Bieseman, and G. Storme, "TomoTherapy: Implications on daily workload and scheduling patients," *Radiother. Oncol.* **86**(2), 224–230 (2008).
31. A. D. Volpe, A. J. M. Ferreri, C. Annaloro, P. Mangili, A. Rosso, R. Calandrino, E. Villa, G. Lambertenghi-Deliliers, and C. Fiorino, "Lethal pulmonary complications significantly correlate with individually assessed mean lung dose in patients with hematologic malignancies treated with total body irradiation," *Int. J. Radiation Oncology Biol. Phys.* **52**(2), 483–488 (2002).
32. S. K. Hui, M. R. Verneris, J. Froelich, K. Dusenbery, and J. S. Welsh, "Multimodality image guided total marrow irradiation and verification of the dose delivered to the lung, PTV, and thoracic bone in a patient: a case study," *Technol. Cancer Res. Treat.* **8**(1), 23–28 (2009).
33. S. J. Cala, C. M. Kenyon, G. Ferrigno, P. Carnevali, A. Aliverti, A. Pedotti, P. T. Macklem, and D. F. Rochester, "Chest wall and lung volume estimation by optical reflectance motion analysis," *J. Appl. Physiol.* **81**(6), 2680–2689 (1996).
34. H. Zhou, Y. Yuan, and C. Shi, "Object tracking using SIFT features and mean shift," *Comput. Vis. Image Underst.* **113**(3), 345–352 (2009).
35. D. N. Ta, W. C. Chen, N. Gelfand, and K. Pulli, "SURFTrac: Efficient tracking and continuous object recognition using local feature descriptors," in *Proc. IEEE Conf. on Computer Vision and Pattern Recognition (CVPR 2009)*, pp. 2937–2944 (2009).